Copyright

IEEE Catalog Number: CFP09ECD-CDR
ISBN: 978-1-4244-2893-9
LOC: 2008935511

Omnipress
2600 Anderson St
Madison, WI 53704
1-800-828-0305

For technical support click here

P2115 Future Home Uninterruptible Renewable Energy System with Vehicle-to-Grid Technology
Igor Cvetkovic, Timothy Thacker, Dong Dong, Gerald Francis, Vladimir Podosinov, Dushan Boroyevich, Fred Wang, Rolando Burgos, Glenn Skut and John Lesko
Virginia Tech, United States and VPT Energy Systems, United States

POSTER SESSION P8-7: APPLICATIONS OF POWER ELECTRONICS AND DRIVES
Chair: M. Pucci, ISSIA-CNR, Italy

P2301 A Novel Electrical Power Supply for Electrothermal and Electrochemical Removal Machining Methods
David Tastekin, Harry Kroetz, Clemens Gerlach and Joerg Roth-Stielow
Universitaet Stuttgart, Germany; ETH Zuerich, Switzerland; SFL GmbH, Germany

P2302 Vector Control of Single-Phase Voltage Source Converters based on Fictive Axis Emulation
Alfred Rufer, Behrooz Bahrani, Stephan Kenzelmann and Luiz Lopes
Ecole Polytechnique Federale de Lausanne, Switzerland; Concordia University, Canada

P2303 A Novel Three-Phase, Switched Multi-Winding Power Electronic Transformer
Ranjan Gupta, Krishna Mohapatra and Ned Mohan
University of Minnesota, United States

P2304 A New Single-phase Voltage Sag/Swell Compensator using Direct Power Conversion
Lee Sanghoey, Cha Hanju and Han Byung-Moon
Chungnam National University, Korea (South); Myongji Engineering University, Korea (South)

P2305 Active Power Transfer Capability of Shunt Family of FACTS Devices Based on Angle Control
Babak Parkhideh and Subhashish Bhattacharya
North Carolina State University, United States

P2306 All Nodes Voltage Regulation and Line Loss Minimization in Loop Distribution Systems Using UPFC
Mahmoud Sayed and Takaharu Takeshita
Nagoya Institute of Technology, Japan

P2307 DPFC Control during the Shunt Converter Failure
Zhihui Yuan, Sjoerd de Haan and Jan Abraham Ferreira
Technical University of Delft, Netherlands

P2308 Evaluation of AFD Islanding Detection Methods Based on NDZs Described in Power Mismatch Space
Xuancai Zhu, Guoqiao Shen and Dehong Xu
Zhejiang University, China

P2309 Control Algorithm for a SSSC with a predictive synchronization algorithm.
Pablo Fernandez-Comesana, Jesus Doval-Gandoy, Francisco Freijedo and Jano Malvar
University of Vigo, Spain

P2310 Digital Control of Switch-mode Pulsed GMAW Welding Power
Dashang Sha and Xiaozhong Liao
Beijing Institute of Technology, China

P2311 Energy Recovery Circuit Using an Address Voltage Source for PDPs
Kang-Hyun Yi, Bong-Chul Kim and Gun-Woo Moon
KAIST, Korea (South)

P2312 A Wide-Speed High Torque Capability Utilizing Overmodulation Strategy for Direct
Auzani Jidin, Nik Rumzi Nik Idris, Halim Yalim and Malik Elbuluk
Universiti of Teknologi Malaysia, Malaysia; University of Akron, United States

P2313 Design Considerations for a Stator Side Voltage Regulated Permanent

P2318 Zero Sequence Circulating Current Control of Interleaved Three Phase Voltage Source Converters with Discontinuous Space Vector Modulation
Di Zhang, Fred Wang, Rolando Burgos and Dushan Boroyevich
Virginia Tech, United States

POSTER SESSION P8-8: PM MACHINES, LINEAR MACHINES AND GENERATORS
Chair: K. Akatsu, Shibaura Institute of Technology, Japan

P1701 Performance Characteristics of an Inverse-Saliency PM Machine in a Vector Control Drive Configuration
Roberto Moncada, Juan Tapia and Thomas Jahns
University of Concepcion, Chile; University of Wisconsin - Madison, United States

P1702 Sensorless Characteristics of Hybrid PM Machines at Zero and Low Speed
Torben Matzen and Peter Rasmussen
Aalborg University, Denmark

P1703 Development of Electric Powertrain with a Boost Converter for the Fuel Cells Plug-in Electric Scooter
Chen-Yen Yu, Ming-Shi Huang and Jung-Ho Cheng
National Taiwan University, Taiwan; National Taipei University of Technology, Taiwan

P1704 Double Channel PM Motor for Avionic Applications: Impact of Winding Topology
Nicolas Velly, Noureddine Takorabet, Farid Meibody-Tabar, Pierre-Yves Liegeois, Florent Nierlich, E.N.Leynaert and G. Humbert
Nancy University INPL - GREEN, France; Messier-Bugatti SAFRAN Group, France

P1705 Comparison of Efficiency for a PI and a FLC Based IPMSM Drive Incorporating Loss Minimization Algorithm Over Wide Speed Range
Mohammad Uddin and Ronald Rebeiro
Lakehead University, Canada

P1706 Stator Design of a Multi-Consequent-pole Bearingless Motor with Toroidal Winding
Ryo Nakamura, Kosuke Kamiya, Akira Chiba, Junichi Asama and Tadashi Fukao
Tokyo University of Science, Japan; Shizuoka University, Japan; Motor Solution Co., Ltd, Japan

P1707 The Shape Design of Interior Type Permanent Magnet BLDC Motor for Minimization of Mechanical Vibration
Gyu-Hong Kang, Jin Hur, Byoung-Kuk Lee and Byoung-Woo Kim
Korea Marine Equipment Research Institute, Korea (South); University of Ulsan, Korea (South); University of Sungkyunkwan, Korea (South); University Ulsan, Korea (South)

P1708 An Improved AC Standstill Method for Testing Inductances of Interior PM Synchronous Motor Considering Cross-magnetizing Effect
Tao Sun, Soon-O Kwon, Jeong-Jong Lee and Jung-Pyo Hong
Hanyang University, Korea (South)

P1709 Lumped Parameter Magnetic Circuit Model for Fractional-Slot Concentrated-Winding Interior Permanent Magnet Machines
Jagadeesh Tangudu, Thomas Jahns, Ayman El-Refaie and Z.Q. Zhu
University of Wisconsin - Madison, United States; GE Global Research Center, United States; University of Sheffield, United Kingdom

P1710 Optimization of a High Force Tubular Linear Drive Concept with Discrete Wound Coils to Fullfill Safety Standards in Industrial Applications
Sebastian Gruber, Christian Junge, Florian Senicar and Stefan Soter
University of Wuppertal, Germany; LTI DRIVES GmbH, Germany; Retrostronik GmbH, Germany

P1711 Design of linear alternators for thermoacoustic machines
Andrea Rossi, Fabio Immovilli, Claudio Bianchini, Alberto Bellini and Giovanni Serra

An Improved AC Standstill Method for Testing Inductances of Interior PM Synchronous Motor Considering Cross-magnetizing Effect

Tao Sun
Hanyang University
Haengdang-dong,
Seongdong-gu
Seoul, 133791, Korea
laplace_sun@hotmail,com

Soon-O Kwon
Hanyang University
Haengdang-dong,
Seongdong-gu
Seoul, 133791, Korea
kso1975@hanyang.ac.kr

Geun-Ho Lee
Hanyang University
Haengdang-dong,
Seongdong-gu
Seoul, 133791, Korea
corleon@hanyang.ac.kr

Jung-Pyo Hong
Hanyang University
Haengdang-dong,
Seongdong-gu
Seoul, 133791, Korea
hongjp@hanyang.ac.kr

***Abstract* -- An inductance measurement method for interior permanent magnet synchronous machine (IPMSM) is proposed in this paper. In this method, the motor is measured at standstill condition, and only a 3-phase voltage source, an oscilloscope and a DC voltage source are required. Depending on the deductive dq-axis voltage equations in the stationary frame of reference, the dq-axis inductances at different current magnetite and vector angle can be calculated by the measured 3-phase voltages and currents. And hence, the saturation and cross-magnetizing effect of the inductances are measurable. This paper introduces the principle equations, experiment setup, data processing, and results comparison on the concentrated-winding and distributed-winding IPMSMs.**

***Index Terms*--Cross-magnetizing effect, Current vector, Inductance measurement, Interior permanent magnet synchronous motors, Standstill experiment method, and Stationary frame of reference.**

I. INTRODUCTION

Interior permanent magnet synchronous motors (IPMSM) have been widely applied in the many fields, such as compressor of house appliance, servo motor of cutting machine, and traction motor of hybrid vehicle, due to their high power density, high efficiency and wide operation range characteristics. Thanks to the finite element method and computer development, many analysis procedures have been successfully used to IPMSM design [1]. However, the experiment methods for verifying the analysis results still have complexity, accuracy, cost and other problems.

Owning to the permanent magnet, salient structure, and rib, the inductance of IPMSM becomes especially difficult to calculate and test [2]. A few numerical methods have been proposed to solve the calculation problem [1]-[4], [7]. The saturation, cross-magnetizing and other effect can be considered and calculated in these methods. There are also several solutions to measure the inductances [2]-[4], [9]. In [9] a method called AC standstill is introduced. This method applies a single phase AC voltage source to one phase motor winding, and measures the currents and voltages of this phase and another phase in order to calculate the self- and mutual-inductances, and further calculate d- and q-axis inductances with them. It is called standstill because the rotor is locked at each test position. It is obvious that the effect of current vector angle varying cannot be reflected, and hence the cross-magnetizing effect is regardless in this method. Additionally, the flux path in two-phase exciting will be different with the one of three-phase exciting. The other standstill method with considering the both saturation and cross-magnetizing effect is introduced in [3]. It fixes the rotor position and uses a vector controller to generate a stepwise d- or q-axis voltage, meanwhile, keep the other axis current constant. According to the current response, the two-axis inductances can be calculated. The difficulty of this method is the generation of the stepwise d- or q-axis voltage. In the ordinary 3-phase inverter, it cannot be directly obtained from the pulse width modulation (PWM) voltage. A high precision low-pass filter must be used. According to phase shift between the flux linkages under the load condition and no-load condition in the steady state, authors of [8] measured the dq-axis inductances in the operation conditions. Keep q-axis current constant, and adjust the load torque so that the total magnitude and vector angle of the load current can be covered. The errors in this method are the unregarded PM demagnetization, and much varying resistance. Based on [8], an improved method is proposed in [4]. In this method, a look-up table is used to correct the error due to the demagnetization of the PM. The complicated and relative expensive system is the shortage of this method. The dynamometer, power meter, vector-control motor drive, low-pass filter, etc. are necessary in order to measure many required variables.

As mentioned above, the methods in [3], [4] and [8] can measure the inductance with considering the cross-magnetizing and saturation effects. When the proper motor drive is absent, however, these inductance test methods become unavailable. In addition, the utilization of dynamometer in [4] and [8] much increases the cost of the experiment system. Considering the practical requirements, this paper proposes a simple method to measure the d- and q-axis inductance of IPMSM. It is based on the AC standstill method, i.e. processed in standstill condition so that the dynamometer is not necessary. It uses a 3-phase AC voltage source so that the vector control drive is not required. It only measures the phase currents and phase voltages, so the power meter is eliminated. Hence, it is very suitable for normal laboratory experiment. The most meaningful point is that this method also can consider the saturation and cross-

magnetizing effect. In this paper, first, the principle of this method will be introduced. And then, based on the deductive equations, the experiment scheme and the processing methods of measured data will be proposed. After briefly introduce the inductance calculation method used in this paper, both a concentrated-winding IPMSM and a distributed-winding IPMSM will be tested and compared with the corresponding calculated results.

II. Improved Standstill Method

In the standstill condition, all measured variables are in the stationary frame of reference. However, the desired d- and q-axis inductances are the variables of the synchronous frame of reference. It is necessary to find the relationship between the measured variables and desired inductances.

A. Inductance in Stationary Frame of Reference

The voltage equation of the IPMSM in the stationary frame of reference is described in (1) [5].

$$\begin{bmatrix} v_q^s \\ v_d^s \end{bmatrix} = \begin{bmatrix} r_s & 0 \\ 0 & r_s \end{bmatrix} \begin{bmatrix} i_q^s \\ i_d^s \end{bmatrix} + \begin{bmatrix} p & 0 \\ 0 & p \end{bmatrix} \begin{bmatrix} \lambda_q^s \\ \lambda_d^s \end{bmatrix}$$
$$\begin{bmatrix} \lambda_q^s \\ \lambda_d^s \end{bmatrix} = \begin{bmatrix} L_q^s & -L_{qd}^s \\ -L_{qd}^s & L_d^s \end{bmatrix} \begin{bmatrix} i_q^s \\ i_d^s \end{bmatrix} + \begin{bmatrix} \lambda_m \sin\theta_{er}^s \\ \lambda_m \cos\theta_{er}^s \end{bmatrix}$$

$$\begin{aligned} L_q^s &= L + \Delta L\cos(2\theta_{er}^s) \\ L_d^s &= L - \Delta L\cos(2\theta_{er}^s) \\ L_{qd}^s &= \Delta L\sin(2\theta_{er}^s) \end{aligned} \tag{1}$$

where r_s is the phase resistance, λ_m is the flux linkage of PM, p represents the d/dt operator, the subscript e represents the unit in electrical angle, $\theta_{er}{}^s$ is the rotor position in stationary frame of reference, and the L and ΔL are calculated by (2).

$$\begin{aligned} L &= \frac{L_q^r + L_d^r}{2} \\ \Delta L &= \frac{L_q^r - L_d^r}{2} \end{aligned} \tag{2}$$

i.e.,

$$\begin{aligned} L_q^r &= L + \Delta L \\ L_d^r &= L - \Delta L \end{aligned} \tag{3}$$

where $L_q{}^r$ and $L_d{}^r$ are the desired q- and d-axis inductances in the synchronous frame of reference.

B. Equations of Measurement Method

(1) also can be expressed as (4),

$$\begin{aligned} v_q^s &= r_s i_q^s + \left(L + \Delta L\cos(2\theta_{er}^s)\right)\frac{d}{dt}i_q^s - 2\omega_{er}^s \Delta L\sin(2v) i_q^s \\ &\quad - \Delta L\sin(2\theta_{er}^s)\frac{d}{dt}i_d^s - 2\omega_{er}^s \Delta L\cos(2\theta_{er}^s) i_d^s + \omega_{er}^s \lambda_m \cos\theta_{er}^s \\ v_d^s &= r_s i_d^s + \left(L - \Delta L\cos(2\theta_{er}^s)\right)\frac{d}{dt}i_d^s + 2\omega_{er}^s \Delta L\sin(2\theta_{er}^s) i_d^s \\ &\quad - \Delta L\sin(2\theta_{er}^s)\frac{d}{dt}i_q^s - 2\omega_{er}^s \Delta L\cos(2\theta_{er}^s) i_q^s - \omega_{er}^s \lambda_m \sin\theta_{er}^s \end{aligned} \tag{4}$$

It is evident that the terms with $\omega_{er}{}^s$ can be eliminated in the standstill condition. And in order to eliminate the sine and cosine terms, the rotor position $\theta_{er}{}^s$ is set to 0^o (or 90^o). Thus the equations are simplified as (5).

$$\begin{aligned} v_q^s &= r_s i_q^s + L_q^r \frac{d}{dt} i_q^s \\ v_d^s &= r_s i_d^s + L_d^r \frac{d}{dt} i_d^s \end{aligned} \tag{5}$$

where the $v_q{}^s$, $v_d{}^s$, $i_q{}^s$ and $i_d{}^s$ are the q- and d-axis voltages and currents. According to the Clarke's transformation in the stationary frame of reference (6), they can be represented by 3-phase voltages and currents that are directly measurable variables. In practice, (5) is modified as (7) in order to satisfy the digital measurement equipment.

$$\begin{bmatrix} f_q^s \\ f_d^s \end{bmatrix} = \frac{2}{3}\begin{bmatrix} 1 & -\frac{1}{2} & -\frac{1}{2} \\ 0 & -\frac{\sqrt{3}}{2} & \frac{\sqrt{3}}{2} \end{bmatrix} \begin{bmatrix} f_a^s \\ f_b^s \\ f_c^s \end{bmatrix} \tag{6}$$

$$\begin{aligned} \left[2v_a(k) - v_b(k) - v_c(k)\right] &= r_s\left[2i_a(k) - i_b(k) - i_c(k)\right] \\ &\quad + L_q^r \frac{\left[2i_a(k) - i_b(k) - i_c(k)\right] - \left[2i_a(k-1) - i_b(k-1) - i_c(k-1)\right]}{T_s} \\ \left[v_c(k) - v_b(k)\right] &= r_s\left[i_c(k) - i_b(k)\right] \\ &\quad + L_d^r \frac{\left[i_c(k) - i_b(k)\right] - \left[i_c(k-1) - i_b(k-1)\right]}{T_s} \end{aligned} \tag{7}$$

where f represents the voltage or current variable, k means the k^{th} value of data, and T_s is the sampling time of the measurement equipment. Finally, in order to express the relationship between the inductances and current vector, the 3-phase current should be converted to the magnitude and angle of the vector in the synchronous frame of reference with Park's transformation (8), (9) and (10).

$$\begin{bmatrix} i_q^r \\ i_d^r \end{bmatrix} = \frac{2}{3}\begin{bmatrix} \cos\theta_{er}^s & \cos(\theta_{er}^s - 120^o) & \cos(\theta_{er}^s + 120^o) \\ \sin\theta_{er}^s & \sin(\theta_{er}^s - 120^o) & \sin(\theta_{er}^s + 120^o) \end{bmatrix} \begin{bmatrix} i_a^s \\ i_b^s \\ i_c^s \end{bmatrix} \tag{8}$$

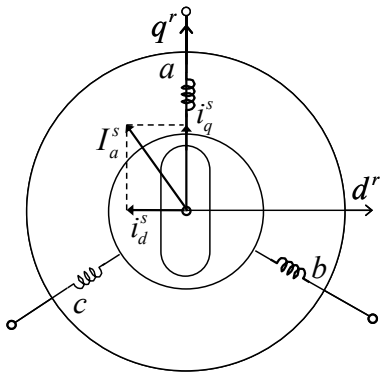

Fig. 1 Relationship between the current vector in stationary frame of reference and standstill synchronous frame of reference

$$I_a = \sqrt{(i_q^r)^2 + (i_d^r)^2} \tag{9}$$

$$\beta = -\arctan\left(\frac{i_d^r}{i_q^r}\right) \tag{10}$$

where $\theta_{er}{}^s$ is 0^o as assumed before, I_a is the magnitude of current vector, and β is the angle of current vector referred to q-axis. As shown in Fig. 1, due to the zero $\theta_{er}{}^s$, the q- and d-axis currents are varying with time. Thus, the measured q- and d-axis inductances cover the various current vector states. Their saturation phenomena can be reflected by different current magnitude, and their cross-magnetizing effect can be measured by the variation of current vector angle.

III. Experiment Devices and Setup

A. Experiment Scheme and Devices

The main purpose of this paper's method is to measure the d- and q-axis inductances considering the saturation and cross-magnetizing effect, and with relatively normal laboratory equipments and simple system. According to the deductive equations, the ideal 3-phase AC voltage source (or current source) is required. Due to desired relationship of current and inductance, the 3-phase AC current source is preferred. In this paper, however, the voltage source will be applied. In the standstill state, there is no back electromotive force (Back-EMF) in each phase. The rated phase current usually can be reached at very low voltage exciting. Therefore, the low voltage range has priority when select the voltage source, in order to increase the precision. In addition, there are current components in the equivalent iron-loss resistances [4], which are not the torque-producing component and rises as the source frequency increasing. Thus relatively low frequency of the AC source also is suggested.

As described in (7), totally there are six variables that should be measured. Unfortunately, more measure channels in oscilloscope implies more expensive price. Due to the asymmetric spatial distribution of phase inductance, there is voltage component in the motor neutral line, i.e. the sum of the 3-phase voltages is no longer zero. Meanwhile, the sum of 3-phase currents always equals to zero. Thus, 3-phase voltage and 2-phase current should be measured. In the case of this paper, a 4-channel oscilloscope is applied. One among the 4channels is used to measure the phase c voltage and phase b current, and combine the two groups of measured data in later manufacture.

In order to find the rotor zero position, a DC voltage generator is used. According to the inverse Clarke's transformation, a d-axis current can be generated by exciting two phase with a DC voltage as shown in (11).

$$\begin{bmatrix} i_a^s \\ i_b^s \\ i_c^s \end{bmatrix} = \begin{bmatrix} 1 & 0 \\ -1/2 & -\sqrt{3}/2 \\ -1/2 & \sqrt{3}/2 \end{bmatrix} \begin{bmatrix} 0 \\ i_d^s \end{bmatrix} = \begin{bmatrix} 0 \\ -i_d^s\sqrt{3}/2 \\ i_d^s\sqrt{3}/2 \end{bmatrix} \tag{11}$$

This d-axis current will align the permanent magnet of one pole with the d-axis. After aligning the zero position, the rotor may be fixed by a vice grid pliers or a brake. Due to the rotation of current vector, it is not necessary to rotate the rotor at each position like the conventional AC standstill method. The experiment Scheme applied in this paper is shown in Fig. 2 (a), while the practice experiment setup is shown in Fig. 3. The total experiment devices include a 50-Hz 3-phase AC source, a 4-channel oscilloscope, a vice grid pliers, and a DC voltage generator. If the proper 3-phase AC voltage source is unavailable, a 3-phase PM synchronous motor with low

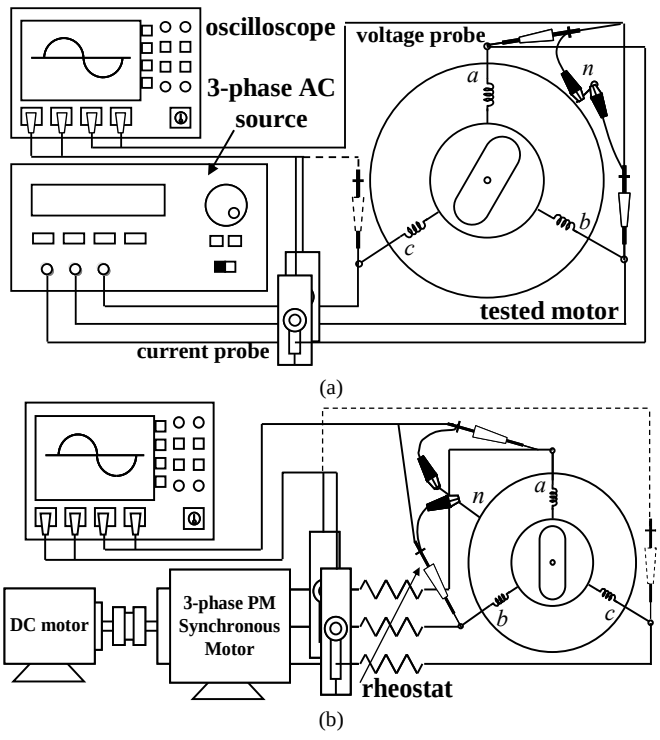

Fig. 2 Experiment setup of inductance measurement: (a) with 3-phase AC source; (b) with 3-phase PMSM

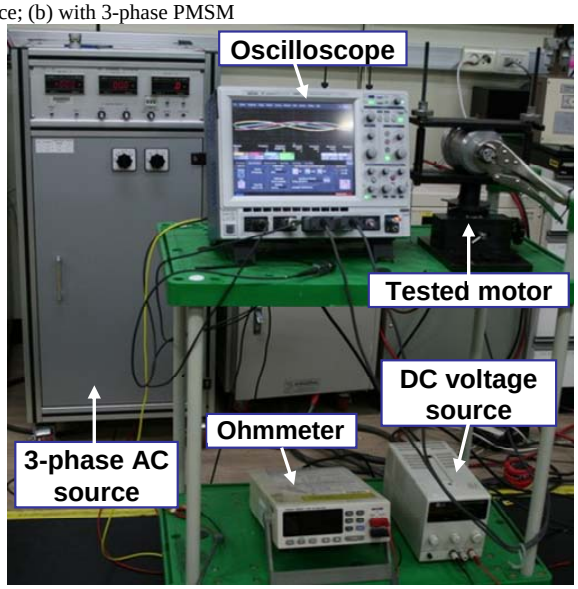

Fig. 3 Experiment setting of inductance measurement in this paper

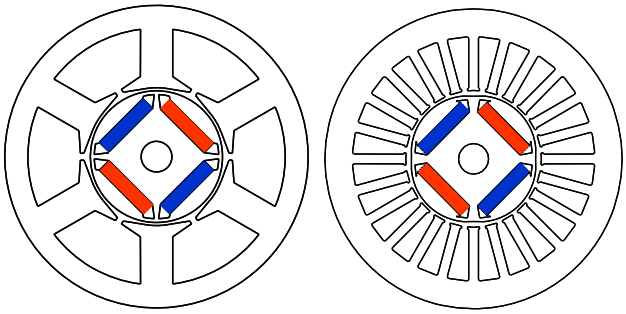

(a) (b)

Fig. 4 Cross-section of test motors: (a) Concentrated winding IPMSM; (b) Distributed winding IPMSM

TABLE I
SPECIFICATION OF CONCENTRATED WINDING IPMSM

Parameters	Value	Unit
Stator outer radii/ Rotor outer radii	80 / 34.5	mm
Airgap length/ Stack length	0.8 / 35	mm
Volume of PM	16×3.5×34	mm^3
Material of core	cogent	
No. of turns in series connected	58	turn
No. of parallel circuits	2	
Phase resistance (@20°C)	0.159	Ohm
Rated current	8.8	A_{rms}

TABLE II
SPECIFICATION OF DISTRIBUTED WINDING IPMSM

Parameters	Value	Unit
Stator outer radii/ Rotor outer radii	80 / 34.5	mm
Airgap length/ Stack length	0.8 / 35	mm
Volume of PM	16×3.5×34	mm^3
Material of core	cogent	
No. of turns in series connected	52	turn
No. of parallel circuits	2	
Phase resistance (@20°C)	0.145	Ohm
Rated current	8.3	A_{rms}

total harmonic distortion (THD) Back-EMF could be used to generate the nearly ideal 3-phase voltage as shown in Fig. 2 (b). In the case of large Back-EMF, the rheostat can be used to reduce the amplitude of the input voltages. And it is better to use the DC voltage generator to drive the traction DC motor rather than a voltage-chopping controller, in order to generate constant frequency.

B. Experiment IPMSM Models

Two IPMSMs with concentrated winding and distributed winding are analyzed and tested in this paper in order to verify the applicability of the proposed method. These two motors are designed for high speed operation. The rated speed reaches 26000rpm. It is difficult to find a proper drive to test this kind of high speed motor. However, the test results will be quite incorrect in the low speed condition due to the influence of the losses components. Therefore, the necessity and advantage of the standstill method appear. The cross-sections of these two motors are shown in Fig. 4 (a) and (b), respectively. And their specifications are shown in Table I and Table II, respectively.

IV. EXPERIMENT DATA AND PROCESSING

A. Experiment Results

In the proposed method, the waveforms of the currents and voltages of the concentrated winding IPMSM and distributed winding IPMSM measured by digital oscilloscope are shown in Fig. 5 (a) and (b), respectively. Because of the different phase inductance in the certain position, it can be seen that the magnitude of the each phase voltage or current is different to the others. These test results are stored as ASCII format data so that the computer program can handle them.

B. FFT Filter for Smoothing Measured Data

The waveforms in Fig. 5 are measured and saved with a digital oscilloscope. The measured voltages and currents hence are discrete-time data. It is obvious that there is much noise in the measured wave forms so that the data cannot be used directly. By means of the Fast Fourier Transform (FFT) filter, the Fourier components whose frequencies are higher than the frequency in (12) can be removed from the original experiment data.

$$f_{threshold} = \frac{1}{n\Delta T} \tag{12}$$

where n is the number of data points considered at one time, and ΔT is the abscissa spacing between two adjacent data points. Fig. 6 shows the comparison between the original data and filtered wave form of phase a voltage.

C. *Ripple Elimination*

Fig. 7 shows the calculated inductance according to the measured phase voltages and currents and deductive formula (7). It can be seen that the raw inductance results have some ripples. The dominate reason is that the slots and teeth of stator produces the different permeability in the spatial distribution. That is also the reason why the inductance curves of the distributed winding IPMSM are smoother than those of the concentrated winding IPMSM. Additionally, due to the asymmetric circuit, the variation of current magnitude and vector angle also may generate different saturation and cross-magnetizing effect. In order to eliminate the ripple of calculated inductances, two methods are proposed in this paper. One is that each current point is tested twice. One time makes the rotor d-axis align to the d-axis of the stationary frame of reference as mentioned previously, the other time rotate rotor d-axis to align q-axis of the stationary frame of reference, i.e. a tooth of stator. Owing to the 90° rotation, the calculated d- and q-axis inductances should be exchanged. Finally, the waveform can be smoothed by solving the mean value of the calculated inductances in the two positions. This method in the theory can reduce the influence of space harmonic components. But both the experiment operation and post data manufacture get much complicated.

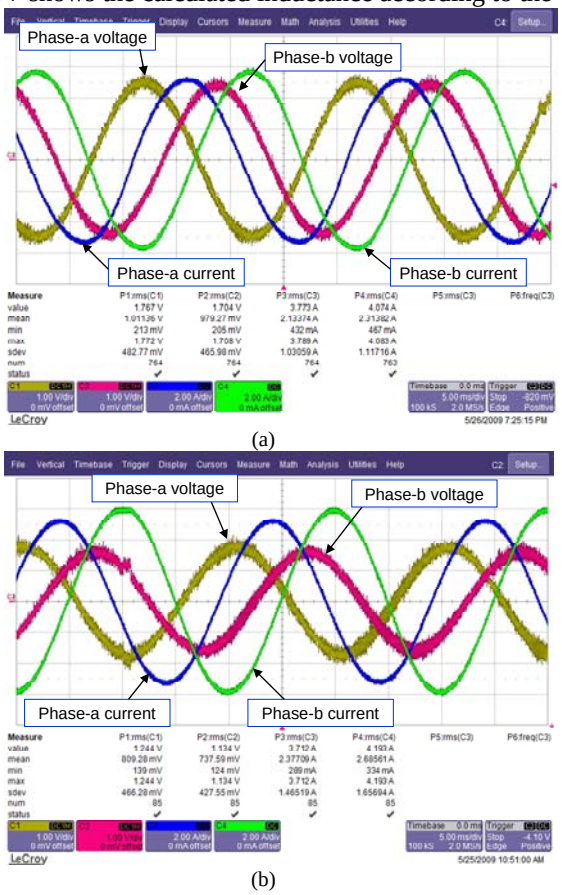

Fig. 5 Measured phase voltages and currents in one period at about 3 A_{rms} : (a) concentrated winding IPMSM; (b) distributed winding IPMSM.

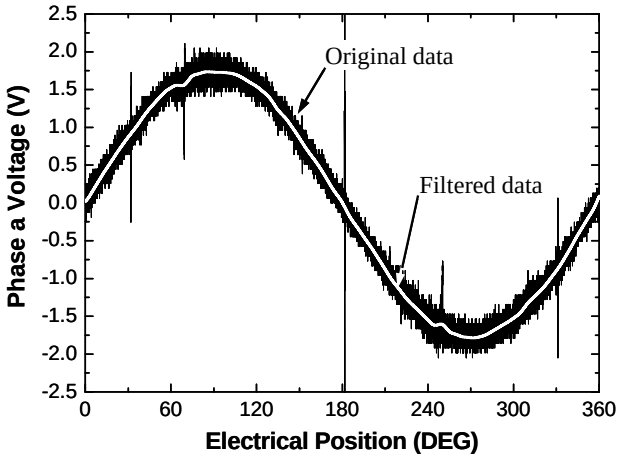

Fig. 6 Comparison of the original data and the filtered data of phase-a voltage waveforms.

The other method is to use the Polynomial Least-square function to fit the curve. The general M-1 orders polynomial least-square function is described in (13).

$$f(x) = a_0 + a_1 x + a_2 x^2 + \ldots + a_M x^{M-1} \tag{13}$$

where a_0, a_1, $a_2 \ldots a_{M-1}$ are chosen to minimize the least-square loss function (14). [6]

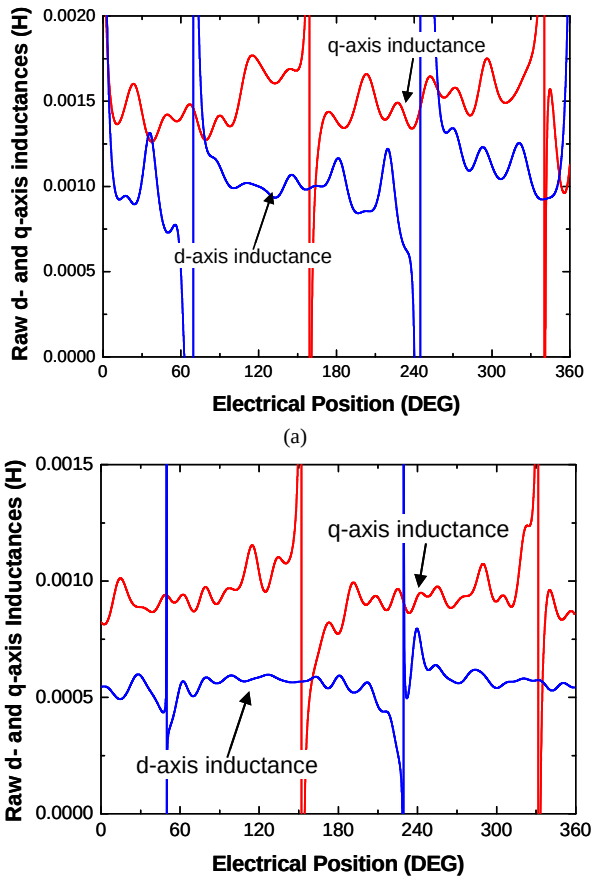

(b)

Fig. 7 Raw measured d- and q-axis inductances at certain voltage: (a) concentrated winding IPMSM; (b) distributed winding IPMSM.

$$\chi^2 = \sum_{i=1}^{N}\left[\frac{y_i - \sum_{k=1}^{M} a_k X_k(x_i)}{\sigma_i}\right]^2 \quad (14)$$

where σ_i is the measurement error of the i[th] data, and N is the number of sampling data.

According to the relationship of current vector angle and electrical position as shown in Fig. 8, the data from 60° to 240° electrical position can cover the current vector angle from the -90° to 90°. Thus, the data in this section is selected and processed by curve fitting. The fitting results of concentrated winding IPMSM and distributed winding IPMSM are shown in Fig. 9 (a) and (b), respectively.

V. Calculation Method

The inductance calculation method used in this paper is introduced in [7]. A phasor diagram of IPMSM is shown in Fig. 10. In the solid-line part, it can be seen that there are the relationships (15) and (16)

$$L_d = \frac{\psi_0 \cos\alpha - \psi_a}{i_d} \quad (15)$$

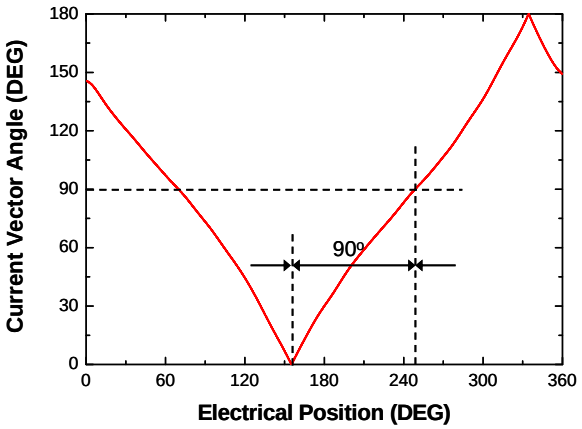

(a)

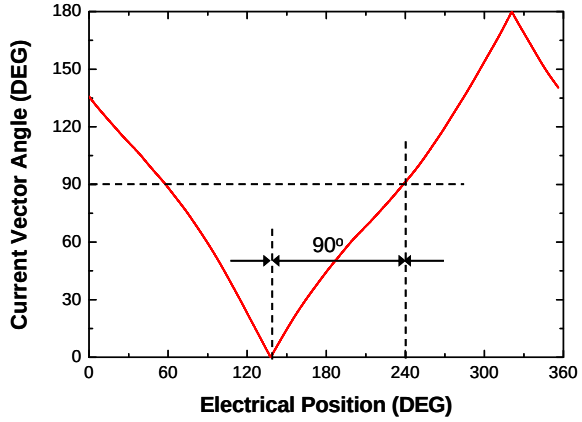

(b)

Fig. 8 Current vector angle: (a) concentrated winding IPMSM; (b) distributed winding IPMSM.

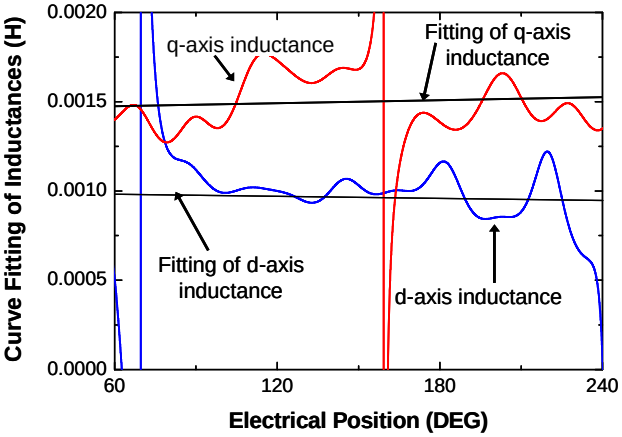

(a)

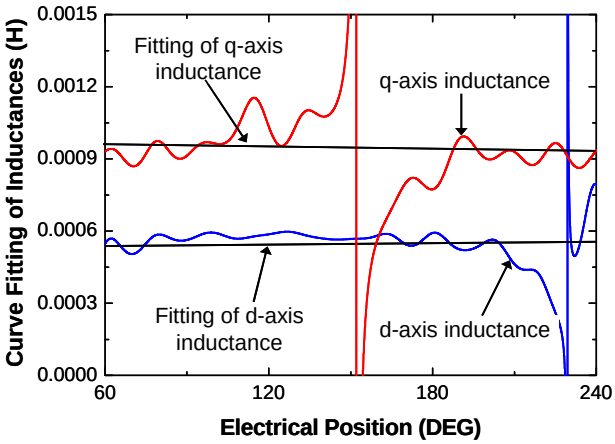

(b)

Fig. 9 Curve fitting of raw inductance results: (a) concentrated winding IPMSM; (b) distributed winding IPMSM.

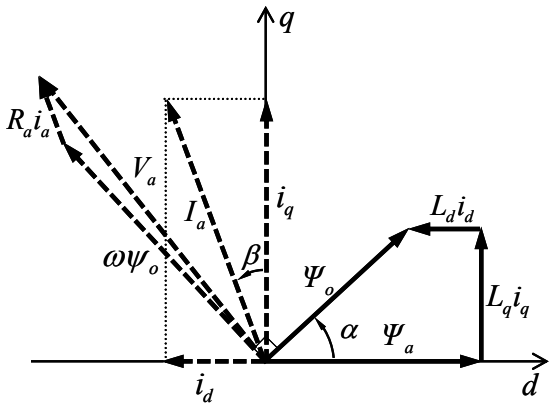

Fig. 10 Phasor diagram of IPMSM

$$L_q = \frac{\psi_0 \sin\alpha}{i_q} \quad (16)$$

where ψ_a is the flux linkage generated by permanent magnet

in no-load condition, ψ_0 is the flux linkage generated by permanent magnet and excited armature current, and the α is the phase shift between the no-load and load Back-EMF

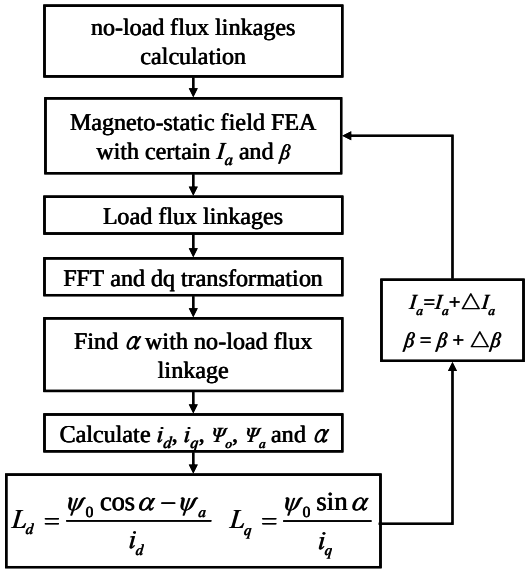

Fig. 11 Procedure of vector control method

According to these equations, an inductance calculation procedure is described in Fig. 11. The detail of this inductance method is introduced in [7].

VI. Comparisons of Results and Discussion

The d- and q-axis inductances of the concentrated winding IPMSM and distributed winding IPMSM calculated by the above method are shown in Fig. 12 (a) and (b), respectively. It can be seen that the inductances of distributed winding IPMSM have no much differences as the current magnitude and vector angle varying, which means the significant cross-magnetizing and saturation effects can not be reflected well. Due to the air cooling method, the current can not reach high. Therefore, the motor always operates under the unsaturated condition.

The d- and q-axis inductances of these two motors measured with the proposed method are shown in Fig. 13 (a) and (b), respectively. Compared with the calculated results, the experimental are very similar to them. It can be seen that the measured d-axis inductances are larger than those of calculation. This is because the rotor d-axis is almost aligned with the stator tooth when find the motor 0^o electrical position and without eliminating the space harmonics. The measured inductances of concentrated winding IPMSM have relatively greater differences with the calculated. As mentioned before, the deductive equations are based on the sinusoidal winding distribution. The concentrated winding generates more space harmonics which strongly influence the accuracy of the principle equations. Additionally, the analysis process does not consider the current components in the iron-loss equivalent resistances. Therefore, larger current is used to produce the flux linkage in the numerical calculation process.

Due to the sinusoidal current wave form, the denominator current terms in (7) may generate the singularity points in the entire electrical period. The measured inductances around these singularity points are strongly distorted, which restricts the measurable inductance range. Hence, it can be seen that there is bullish trend near the 80^o in the tested d-axis inductance. However, the simplicity and acceptable accuracy make this method be a prefer choice in some situation.

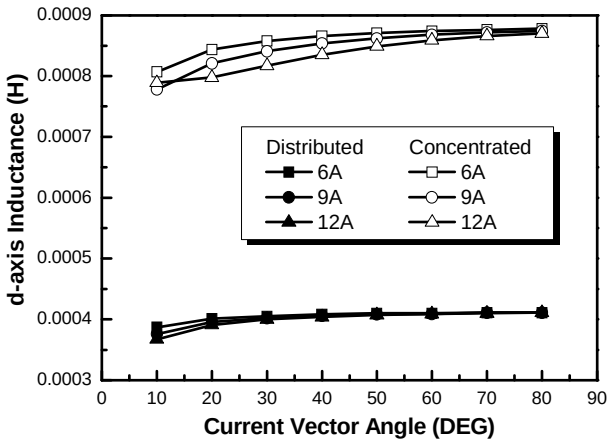

(a)

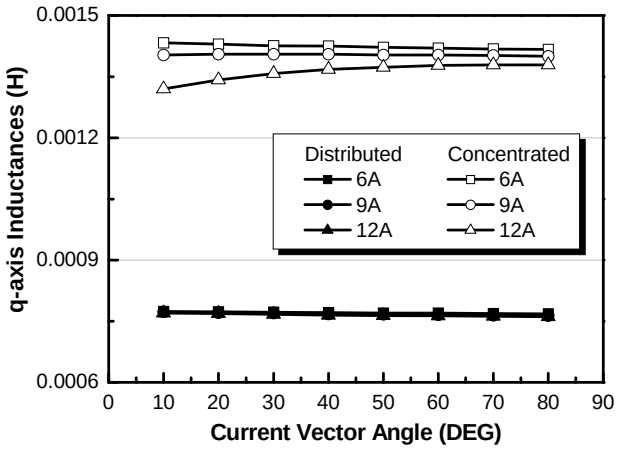

(b)

Fig. 12 Calculated inductances: (a) d-axis inductances; (b) q-axis inductances

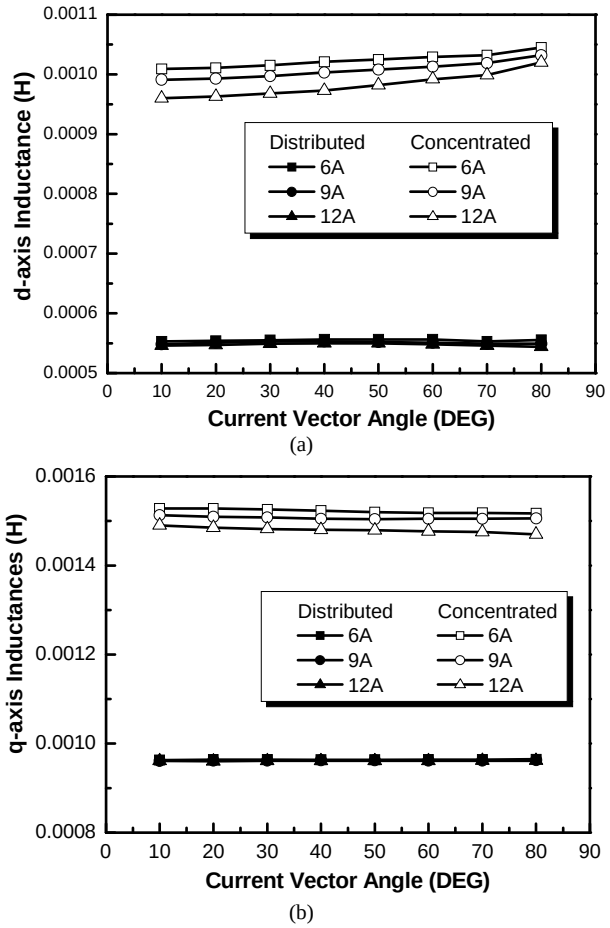

Fig. 13 Measured inductances: (a) d-axis inductances; (b) q-axis inductances

VII. CONCLUSION

The d- and q-axis inductance calculation and measurement are very important to the performance prediction and optimal control of IPMSM. Several measurement methods have been proposed in the previous literatures. However, the inherent drawback or complicated system configuration lead these methods are not always available. Based on this problem, this paper proposed a simple experiment method to measure the d- and q-axis inductance of IPMSM in the stationary reference frame. After a series of data processing, the d- and q-axis inductances reflecting cross-magnetizing and saturation effects can be obtained. Compared with the calculated results, the inductances measured in this method are reliable, especially for the distributed winding motor. Further, the principle equations will be deducted with account for the space harmonics of concentrated winding.

REFERENCES

Periodicals:

[1] J. Y. Lee, S. H. Lee, G. H. Lee, and J. P. Hong, "Determination of parameters considering magnetic nonlinearity in an interior permanent magnet synchronous motor," *IEEE Trans. Magn.*, Vol. 42, No. 4, Apr. 2006.

[2] R. Dutta, and M. F. Rahman, "A comparative analysis of two test methods of measuring d- and q-axis inductances of interior permanent magnet machine," *IEEE Trans. Magn.*, Vol. 42, No. 11, Nov. 2006.

[3] B. ˇStumberger, G. ˇStumberger, D. Dolinar, A. Hamler, and M. Trlep, "Evaluation of saturation and cross-magnetization effects in interior permanent-magnet synchronous motor," *IEEE Trans. Ind. Appl.,* Vol. 39, No. 5, Sept./Oct. 2003.

[4] K. M. Rahman and S. Hiti, "Identification of machine parameters of a synchronous motor, " *IEEE Trans. Ind. Appl.,* Vol. 41, No. 2, Mar./Apr. 2005.

[5] G. D. Andreescu, C. I. Pitic, F. Blaabjerg, and I. Boldea, "Combined Flux Observer With Signal Injection Enhancement for Wide Speed Range Sensorless Direct Torque Control of IPMSM Drives," *IEEE Trans. Energy Conv*., vol.23. no. 2,pp.393-402, June. 2008.

Books:

[6] W. H. Press, etc., *Numerical Recipes in C: The Art of Scientific Computing 2nd edition.* Cambridge University Press, Oct. 1992.

Papers from Conference Proceedings (Published):

[7] T. Sun, S. O. Kwon, S. H. Lee, and J. P. Hong, "Investigation and Comparison of Inductance Calculation Methods in Interior Permanent Magnet Synchronous Motors, " in Proc. 2008 IEEE *Electrical Machines and Systems, Conf.*, pp. 3131-3136.

[8] E. C. Lovelace, T. M. Jahns, J. Wai, T. Keim, J. H. Lang, D. D. Wentzloff, F. Leonardi, J. M. Miller, "Design and experimental verification of a direct-drive interior PM synchronous machine using a saturable lumped-parameter model," in Proc. 2002 IEEE *Ind. Appl. Conf.,* Vol. 4, pp. 2486-2492.

Standards:

[9] *IEEE Standard Procedure for Obtaining Synchronous Machine Parameters by Standstill Frequency Response Testing*.,IEEE Standard 115A-1987, 1987